Research Article

Jing Gong, Yi Qian, Ziyang Xu*, Chaoqian Chen, Yijing Jin, Junze Zhang, Zhipeng Li*, and Xianming Shi

Effect of graphene oxide on the properties of ternary limestone clay cement paste

https://doi.org/10.1515/ntrev-2023-0222
received June 14, 2023; accepted February 22, 2024

Abstract: Given the pressing threat of global warming, it is imperative to promote CO_2 emission reduction within the cement industry which is widely recognized as a major contributor to the overall carbon footprint. Limestone clay cement (LCC) emerges as a promising alternative to Portland cement. However, to facilitate the implementation of LCC technology, it is urgent to address the low early-age compressive strength issue. Inspired by the successful implementation of nano-engineered cementitious material, we hereby introduce a novel nanomaterial, graphene oxide (GO), into unconventional LCC paste (cement: clay:limestone = 65%:20%:15%, water/binder ratio: 0.45). Experimental results revealed that the 0.09% GO by weight of the LCC binder was the optimal dosage in this work, which improved the compressive strength of the LCC paste at 7, 14, and 28 days by 25.6, 21.6, and 20.3%, respectively. Advanced characterizations were then conducted, suggesting that the admixed GO not only enabled a higher polymerization degree of binder hydrates (which benefited the development of compressive strengths) but also improved the carbonation resistance of LCC paste. These findings not only offer valuable insights for researchers but also provide practical guidance for engineers in the field. Notably, the admixed GO converted the unstable orthorhombic crystal systemic aragonite to the stable trigonal crystal systemic calcite, which offers insights into the technology of carbon sequestration in concrete.

Keywords: limestone clay cement, graphene oxide, compressive strength, degree of polymerization, carbonation resistance, Fourier-transform infrared spectroscopy analysis

1 Introduction

Recent years have seen increasing concerns over the environmental footprint of the concrete industry, especially its considerable CO_2 emission and energy consumption [1], largely associated with the production of ordinary Portland cement (OPC). According to the global carbon emission report, the CO_2 emission from the concrete industry is estimated to be about 8% of the total CO_2 emission [1]. The emitted CO_2 will result in an irreversible greenhouse effect and ultimately pose a significant risk to the ecosystem. Therefore, there is an urgent need to reduce the carbon emissions from the cement and concrete industries.

Limestone calcined clay cement (LC^3) has emerged as a promising candidate to reduce the environmental footprint of the cement and concrete industries [2,3]. LC^3 is a ternary blended cement consisting of calcined clay, limestone, and OPC, and saves up to 40% of CO_2 and 20% of energy consumption as compared with conventional OPC [2]. In this ternary system, the limestone (carbonate phase) reacts with alkali and alumina derived from the hydration of OPC to generate hard and crystalline carboaluminate phases which significantly contribute to the development of the microstructure [4]. Additionally, the calcined clay displays promising pozzolanic reactivity, actively promoting the hydration process. Moreover, some of the limestone effectively fills the hydrate pores, contributing to the densification of the microstructure [3]. The synergistic effects of these three components make it possible to decrease the

* **Corresponding author: Ziyang Xu,** School of Civil Engineering and Architecture, Wuhan Polytechnic University, Wuhan, 430023, China, e-mail: Ziyang__xu@163.com
* **Corresponding author: Zhipeng Li,** National Center for Transportation Infrastructure Durability & Life-Extension, Department of Civil & Environmental Engineering, Washington State University, P.O. Box 642910, Pullman, WA, 99164-2910, United States of America, e-mail: zhipeng.li2@wsu.edu, li_zhipeng@hotmail.com
Jing Gong: School of Civil Engineering and Architecture, Wuhan Polytechnic University, Wuhan, 430023, China; Intelligent Construction College, Wuchang University of Technology, Wuhan, 430223, China
Yi Qian, Chaoqian Chen, Yijing Jin, Junze Zhang: School of Civil Engineering and Architecture, Wuhan Polytechnic University, Wuhan, 430023, China
Xianming Shi: National Center for Transportation Infrastructure Durability & Life-Extension, Department of Civil & Environmental Engineering, Washington State University, P.O. Box 642910, Pullman, WA, 99164-2910, United States of America

cement content while retaining the satisfactory performance of the hardened LC^3 binder [2]. In addition, both clay and limestone are affordable and locally available, making the widespread application of LC^3 much more feasible than many other types of alternative cementitious binders (*e.g.*, supplementary cementitious material [SCM] cement and SCM-based geopolymer) [5,6]. Nevertheless, the utilization of LC^3 requires the grinding of clinker with calcined clay and limestone, a process that may face limitations due to the limited availability of local cement plants with the necessary infrastructure for such grinding. Therefore, we introduced calcined clay and limestone in combination as a mineral additive and investigated the performance of this limestone clay cement (LCC) ternary composite, differentiated from the aforementioned LC^3 composite.

LCC binders have been previously explored and have demonstrated significant potential for local construction. For example, Antoni *et al.* [7] employed a ternary binder consisting of 30% metakaolin, 15% limestone, and 55% OPC, which exhibited promising mechanical properties suitable for construction applications. Additionally, Drissi *et al.* [8] investigated the relationship between the composition of ternary OPC–metakaolin–limestone composites and their hydration, microstructure, and mechanical properties, contributing significantly to both scientific understanding and engineering practice. However, the relatively low early-age compressive strengths of LCC composites hinder the widespread application of this sustainable technology [9]. Therefore, finding an alternative method to improve their mechanical strength while maintaining a lower OPC dosage is of paramount importance to ensure their sustainability.

Cumulative studies have demonstrated the feasibility of admixing a trace amount of novel graphene oxide (GO) to greatly enhance various cementitious materials [10–12]. As a nascent nano-sized material, GO is originally derived from graphite through a strong oxidization process (*e.g.*, Hammer's method) [13]. The oxidization process not only exfoliates the layers of graphite but also grafts functional groups onto the surface of GO nanosheets, and these include, but are not limited to, carboxyl, hydroxyl, epoxide, and carboxylic groups [14]. The functional groups endow the GO with an electronegative surface charge, which plays a crucial role in the hydration process of cementitious materials. Generally, the electronegative GO serves to fill nanoscale pores, bridge and deflect microcracks, attract electropositive ions (*e.g.*, Ca^{2+}, Na^{+}, and K^{+}), and regulate the process of binder hydration to form better products [15,16]. More importantly, these functional groups endow GO with a higher level of hydrophilicity than other nanomaterials. In other words, GO can be dispersed more easily without requiring significant additional effort, making it a promising candidate among the various nanomaterials reported in previous studies aimed at enhancing cementitious composites. Furthermore, recent advances in large-scale manufacturing of GO have led to the exponential decline of the cost of GO, making it greatly more affordable than before. Our previous research has demonstrated the benefits of admixing 0.02 wt% GO in the OPC binder [17] and a fly ash-based geopolymer binder [11], respectively, inspiring the beneficial use of GO in this unconventional LCC binder.

Up to now, limited studies have investigated the effect of admixing GO on the LCC composites, yet we hypothesized that GO plays similar roles in LCC binder as it works in OPC and geopolymer binders and thus benefits the early-age compressive strengths of LCC paste. In this context, this work aimed to enhance the early-age compressive strengths of LCC paste specimens by incorporating GO. To test the aforementioned hypothesis, we employed scanning electron microscopy (SEM), thermogravimetric analysis (TGA), X-ray diffraction (XRD), and Fourier transform infrared spectroscopy (FTIR) to shed light on the influence of GO on the microscale characteristics of the LCC paste. The following sections detail the experimental design, sample preparation, performance testing, and advanced characterizations of the GO-LCC paste. This innovative composite material holds promise for a wide range of engineering applications (*e.g.*, low-carbon concrete pavement) and the fundamental understanding from this research helps inform future research and application.

2 Experimental study

2.1 Materials

This study used P.O.42.5 OPC as purchased from Foshan Runhe Building Materials Co., Ltd. The limestone (calcite) and calcined clay (98 wt% metakaolin) were produced by Henan Borun Casting Materials Co., Ltd. The chemical composition of cement and metakaolin was examined by X-ray fluorescence, the chemical composition of limestone was provided by the producer, and all results are provided in Table 1. XRD analysis was also performed on the cement and metakaolin to reveal their crystalline mineral phases (Figure 1). As seen in Figure 1, the main crystalline phases in the cement were C_3S, C_2S, C_3A, and C_4AF, while kaolinite was dominant in the calcined clay. In addition, the specific surface area of cement, limestone, and metakaolin was 363, 475, and 17,000 m^2/kg, respectively. The naphthalene superplasticizer provided by Shunxin Huagong (Jinan, China) was employed in this study to guarantee the flowability of LCC paste. The water reduction rate of this superplasticizer

Table 1: Chemical composition (wt%) content of materials

Chemical composition	Cement	Limestone	Calcined clay
Al_2O_3	4.12	—	37.18
SiO_2	20.50	0.40	57.81
Fe_2O_3	3.40	—	1.19
CaO	65.54	0.66	0.88
MgO	2.61	1.12	—
SO_3	0.52	0.18	0.58
$K_2O + Na_2O$	0.78	0.43	0.72
TiO_2	—	—	1.39
$CaCO_3$	—	97.21	—
LOI*	2.53	—	0.25

*The loss on ignition was determined by TGA.

was 18–28% and its recommended dosage for OPC was 0.5–1%, as provided by the manufacturer.

Based on previous exploration, the LCC binder investigated in this study consists of 65 wt% cement, 20 wt% metakaolin, and 15 wt% limestone. The GO employed in this study was fabricated using a modified Hammer's method in the laboratory [13], featuring a specific surface area of about 2,600 m^2/g and no more than five layers of nanosheet (Figure 2a). This GO contained about 71 wt% carbon, 26 wt % oxygen, and some other elements from the oxidation process [18,19], and its main functional groups/chemical bonds were C–OH, C–C, and C═O bonds (Figure 2b).

2.2 Specimen preparation

The GO-LCC paste samples were fabricated in the laboratory as follows. The dosage of admixed GO was designed as 0, 0.045, 0.09, 0.135, and 0.18% by the weight of the LCC binder, respectively (Table 2). The water-to-LCC mass ratio was fixed at 0.45. First, the laboratory-fabricated GO and naphthalene superplasticizer (1 wt% to LCC) were ultrasonically dispersed in deionized water, with the ultrasonicator power of 40 W for 30 min to obtain desirable dispersion. Then, the fabricated GO solution (or aqueous suspension when exceeding 5 g/L) was poured into a 2.5 L mixer, followed by blending with limestone (15 wt%), metakaolin (20 wt%), and cement (65 wt%) in sequence with 1 min intervals. During the intervals and the mixing process, the mixer was kept at a slow but constant blending rate (*i.e.*, 60 rpm). After mixing the LCC cement for another 1 min, the fresh paste was cast into cubic molds (70.7 mm × 70.7 mm × 70.7 mm) and then cured in a standard environment (temperature of 18–22°C, relative humidity of 95–98%). After 24 h of curing, these paste samples were demolded and then cured in the same condition for 6, 13, and 27 days in order to evaluate the compressive strength of the hardened LCC paste at 7, 14, and 28 days, respectively. The fabrication of A0 followed the same procedure but without GO.

2.3 Macroscopic testing

The macroscopic testing included compressive strength and flowability tests, aimed at assessing the impact of GO on general practical engineering performance. By following the ASTM C109, the compressive strength of cubic specimens (50 cm × 50 cm × 50 cm) was conducted using an electro-hydraulic servo compression test machine with a loading speed of 0.1 MPa/s. The peak load was recorded to calculate

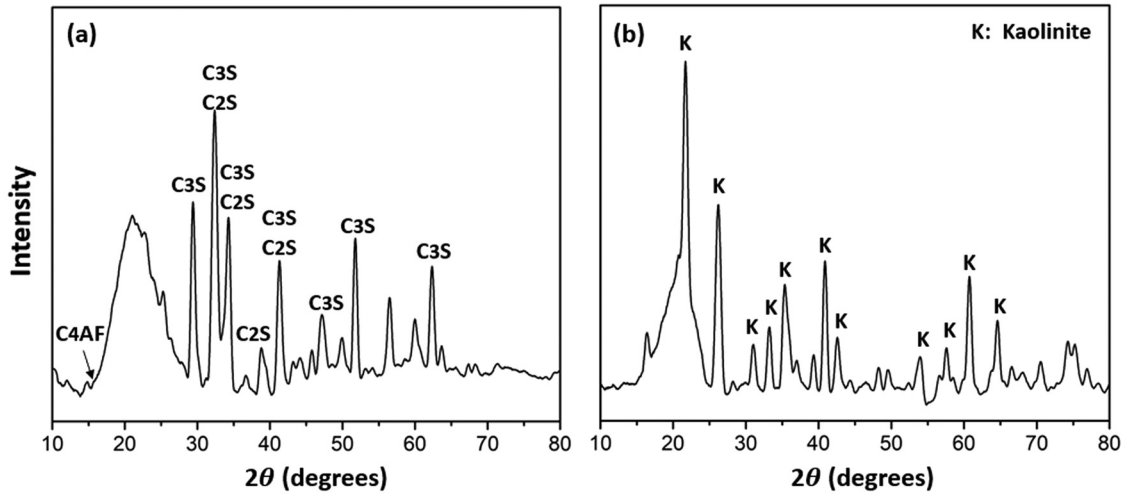

Figure 1: XRD patterns of (a) OPC and (b) metakaolin.

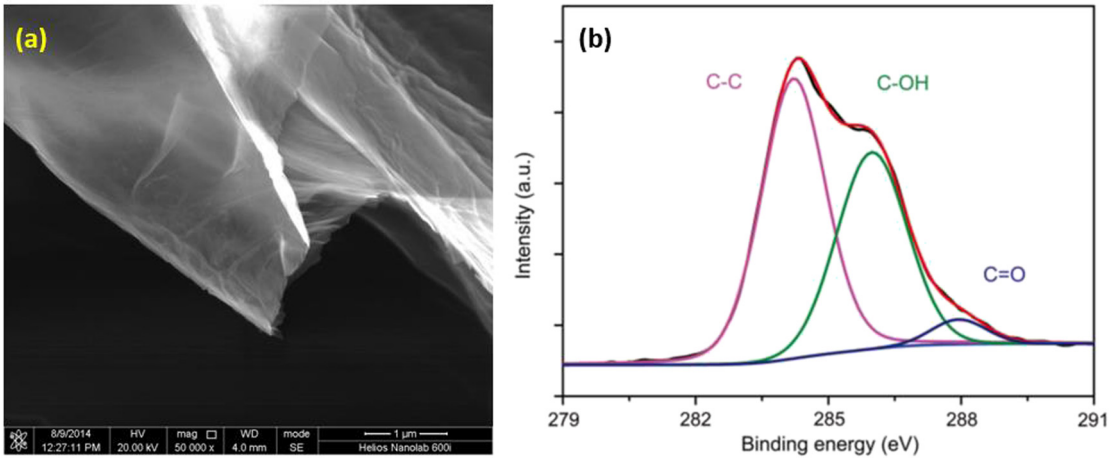

Figure 2: (a) Micromorphology of GO nanosheet and (b) X-ray photoelectron spectroscopy analysis of GO [18,19].

Table 2: Mixture design of GO-LCC paste samples (g)

No.	Cement	Limestone	Metakaolin	Water	GO	Superplasticizer
A0	845	195	260	585	0	13
A1					0.585	13
A2					1.17	13
A3					1.755	13
A4					2.34	13

the compressive strength, and the final result was reported as the average value of three measurements. Flowability assessment utilized a 50 mL beaker to simulate the mini-slump test, following the methodology outlined in Li and Shi's study [11]. In this procedure, the fresh paste was poured into the beaker, then covered and inverted with a wet plastic plate. The beaker was subsequently raised vertically, allowing measurement of the diffused diameter, which was used to evaluate the flowability among distinct paste samples. Four pairs of perpendicular diameters were gauged, and their average was employed for comparative analysis, as detailed in Figure 3.

2.4 Microscopic investigations

This study entailed microscopic investigations designed to unravel the mechanistic roles of the admixed GO on the hydration of LCC paste. Before the analysis, the selected paste samples were dried at 50°C to remove the remaining moisture. The XRD analysis was performed using a D/max-2500 facility (Rigaku company, Japan) to investigate the effect of GO on the crystalline phases in the LCC hydration system. For the XRD analysis, the tube voltage was set at 40 kV, the tube current was set at 200 mA, the scanning range was set between 10° and 80°, and the scanning speed was set at 10°/min. The SEM analysis was conducted using a Hitachi S-4800 facility (HITACHI Company, Japan) to investigate the effect of GO on the microstructure and micromorphology of LCC hydration products. For the SEM, the selected samples were pre-coated with gold before analysis, the accelerating voltage was set as 15 kV and the probe current was set as 22 nA. The FTIR analysis was conducted using a Nicolet iS5 facility (Jingong Instrument Technology (Suzhou) Co., Ltd, China) to investigate the effect of GO on the chemical groups or bonds of LCC hydration products. For the FTIR, powdered paste samples were well-mixed with KBr in the mass ratio of 1:100 and then fabricated plates for analysis, the scanning range was between 400 and 4,000 cm^{-1} with a resolution of 4 cm^{-1}. The TGA and corresponding differential thermogravimetry (DTG) study were performed by a Q2000 facility (TA Instrument, USA) to investigate the effect of GO on the chemical composition of LCC hydration products. For the TGA, the powdered paste samples were pre-heated at 50°C for 10 min to remove the remaining moisture and then heated up for analysis, the initial and ending temperature was set as 50 and 800°C, respectively, at a heating rate of 10°C/min.

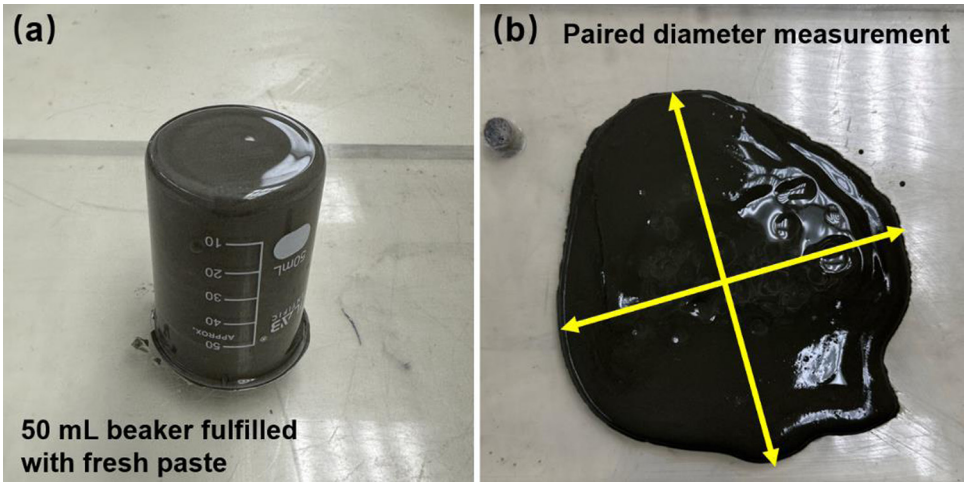

Figure 3: (a) 50 mL beaker filled with fresh paste and (b) demonstration of one pair of perpendicular diameter measurements of the diffused fresh paste.

3 Results and discussion

3.1 Compressive strength

The admixed GO significantly improved the compressive strength of LCC paste (as shown in Figure 4); in particular, the 0.09 wt% GO improved the compressive strength of the LCC paste at 7, 14, and 28 days by 25.6, 21.6, and 20.3%, respectively, working as the optimum dosage among all designed dosages. Our previous work reported similar results, in which the 0.02% GO (by weight of cementitious binder) improved the 7-day and 28-day compressive strength of a fly ash-based geopolymer paste by 6 and 9% [11], and improved the 7-day, 14-day, and 28-day compressive strength of a cement paste by 34, 27, and 29% [17], respectively. Other researchers have also reported similar trends. Pan *et al.* [18] reported that admixing 0.05 wt% GO increased the compressive strength and flexural strength of cement paste at 28 days by 15–33% and by 41–59%, respectively. Lv *et al.* [20] reported that admixing 0.05 wt% GO led to the highest 28-day compressive strength of an OPC mortar, featuring an increase of 48%. The different levels of strength improvement observed across these studies are due to the differences in the cementitious binder matrix. Furthermore, Lin *et al.* reported the 12.5 and

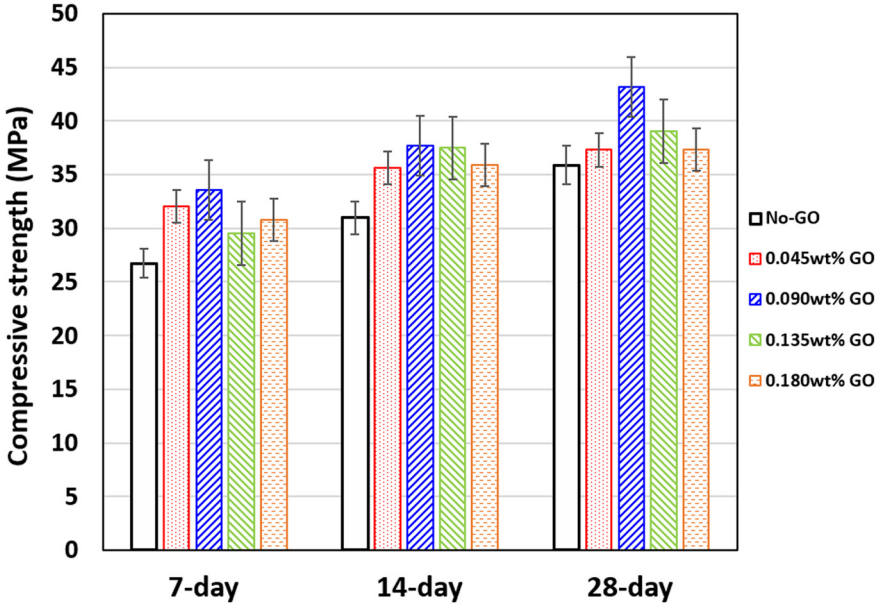

Figure 4: Effect of admixed GO on the compressive strength of LCC paste.

28.2% increase in the 28-day compressive strength by incorporating 1 and 2 wt% nano-silica to enhance the LC^3 binder [21], respectively. This finding not only underscores the advantages of utilizing nanomaterials but also serves as an inspiration for enhancing unconventional limestone–cement–clay binders.

When the dosage of GO exceeded 0.09 wt%, however, the benefits of admixed GO to the compressive strength of the LCC paste declined, as illustrated in Figure 4. This is likely due to poor dispersion and thus undesirable agglomeration of GO that undermines the homogeneity of the LCC paste matrix. Although GO is hydrophilic, the GO nanosheets feature a considerably high specific surface area; as such, a high concentration of GO nanosheets in the concrete pore solution tends to agglomerate with each other, because of the presence of Van der Waals force [5,22] and possibly hydrogen bonding. Additionally, the accelerated hydration induced by GO, as explained in later sections, in the LCC binder results in reduced flowability, consequently exerting a detrimental impact on the consolidation of fresh paste. In other words, it introduces pores into the hardened paste and reduces its compressive strength. Similar mechanisms have been widely reported in nano-modified cementitious materials [23,24].

The beneficial effects of GO on the compressive performance of non-LCC cementitious composites have been widely discussed and accepted in the last few years [22,25]. The admixed GO works against crack propagation in the cementitious composite, due to the GO's sheet-like structure (Figure 2a) and excellent mechanical property (290–430 GPa of the elastic modulus). Furthermore, the admixed GO benefits the hydration of cementitious binders through several mechanisms. The known mechanisms of this improvement include the nano-filling, microcrack bridging and deflecting, hydrates growth template, hydration acceleration, and hydration regulation roles played by GO. The following sections will focus on the microstructural morphology, chemical composition, and crystalline phases of selected GO-LCC paste samples to confirm the aforementioned roles played in GO in the LCC matrix.

3.2 Flowability

The admixed GO resulted in decreased flowability of fresh LCC paste, particularly noticeable when the GO dosage exceeded 0.135 wt% (as shown in Table 3). Despite metakaolin's recognized high water absorptivity, the relatively increased amount of water-reducing agent and elevated water-to-binder ratio offset the metakaolin-induced decline in flowability. Furthermore, the addition of GO caused a reduction in flowability, consistent with the findings from previous researchers. For instance, Lu *et al.* demonstrated a 24% decrease in fluidity with 0.08 wt% admixed GO [25], while Li and Shi reported a reduction in diffused area from 161.4 mm × 156.76 mm to 139.8 mm × 136.6 mm with 0.02 wt% admixed GO [11]. This reduction is often attributed to GO's extensive specific surface area and high surface reactivity, leading to boosted water absorption and subsequently diminished flowability. The same principle can explain the flowability reduction observed in this study. The GO-accelerated hydration process is another crucial factor contributing to the decreased fluidity. Due to limitations in the laboratory conditions, the hydration heat of each binder was not evaluated in this study. Nevertheless, findings from other studies support this perspective. For example, in Lin *et al.*'s research, the addition of nano-silica resulted in a significantly higher cumulative hydration heat in the first 15 h than the original LC^3 and OPC binders, indicating the accelerated hydration induced by nanomaterials. An *et al.* [26] also reported that GO-modified OPC released more cumulative hydration heat in the first 20 h, further demonstrating GO's role as a hydration accelerator in cementitious binders.

Comparing the A1 and A2 specimens with paste A0 (without GO), although their flowability decreased but remained within acceptable limits; as such, they still could be easily compacted through vibration during practical applications. Conversely, the A3 and A4 specimens experienced substantial flowability losses, rendering them difficult to compact. The compromised flowability facilitated the formation of entrapped air voids, contributing to a porous macrostructure in A3 and A4, which is a contributing factor to the slightly reduced compressive strength.

3.3 FTIR and XRD analyses of hydrates

FTIR analysis was conducted to illustrate the influence of GO on the phase change, product formation, and chemical arrangement in the hydrated LCC paste. As shown in Figure 5a. The −OH bond detected at around 3,640 cm^{-1} could be attributed to the presence of portlandite, derived

Table 3: Mean and standard deviation of flowability for each fresh LCC paste (mm)

Sample	A0	A1	A2	A3	A4
Flowability	181(10)	163(8)	129(9)	73(8)	53(7)

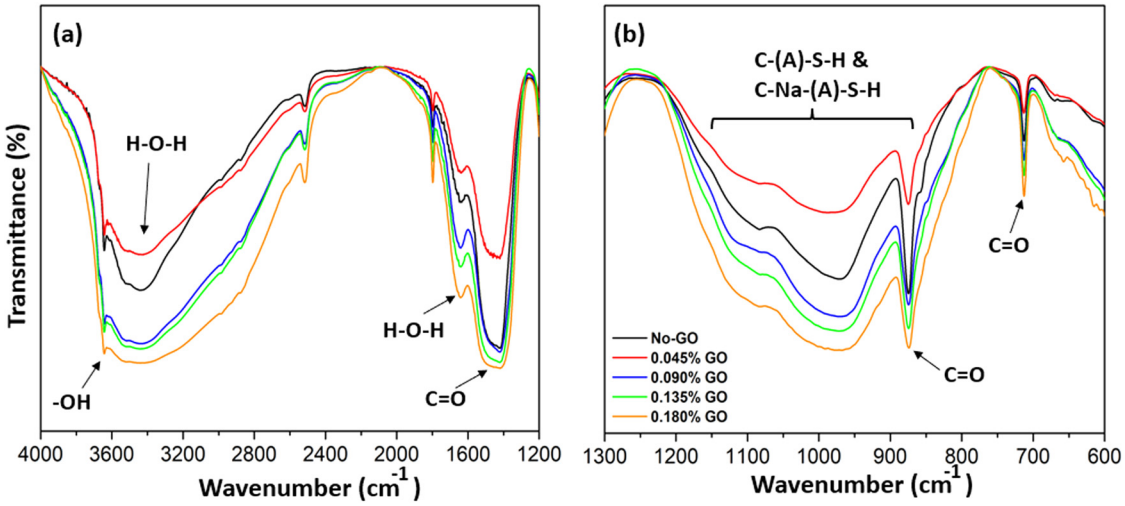

Figure 5: FTIR patterns of selected GO-LCC paste samples from (a) 1,200–4,000 cm^{-1} and (b) 600–1,300 cm^{-1} wavenumber length.

from the hydration of cement [27]. The H–O–H broad band centered at around 3,400 and 1,640 cm^{-1} can be ascribed to the presence of bound water in hydration products [28]. The C═O stretching detected at around 1,410 cm^{-1} (asymmetric C═O stretching) in Figure 5a, 875 cm^{-1} (out-of-plane bending), and 713 cm^{-1} (in-plane vibration) in Figure 5b could be ascribed to the presence of both carbonated hydrates and mixed limestone [29]. These chemical compositions were also confirmed by TGA/DTG analysis in a later section.

The in-depth analysis of FTIR data suggests that the admixed GO improved the polymerization degree of binder hydrates, which is consistent with the compressive strength results and the later SEM analysis of the LCC paste. Figure 6 depicts the deconvolution analysis of FTIR from 750 to 1,250 cm^{-1}, and Figure 7 summarizes the relative area of these deconvoluted sub-peaks. The deconvolution of FTIR sub-peaks in Figure 6 followed the methodology detailed by Zhang *et al.* [30], and the results illustrate the influence of GO on the critical hydrates (*e.g.*, C–(A)–S–H and C–Na–(A)–S–H) in the hydrated LCC paste. In general, Q^0 represents the cement monomer, Q^1 represents the Si–O tetrahedron located at the end of the C–S–H chain, Q^2 represents the Si–O tetrahedron located in the middle of the C–S–H chain, Q^3 represents the Si–O tetrahedron in the C–S–H network, and Q^4 represents the Si–O tetrahedron in the quartz structure [23]. In this study, the sub-peak located at around 865 cm^{-1} was assigned to Si–O terminal vibrations in C–S–H/C–A–S–H gel (a.k.a., Q^1 tetrahedron), the sub-peak at around 962 cm^{-1} was assigned to Q^2 tetrahedron, the sub-peak at around 1,026 cm^{-1} was assigned to Si–O stretching in C–Na–(A)–S–H gel which was ascribed to the binding of Na onto C–(A)–S–H gel, the sub-peak at 1,097 cm^{-1} was assigned to Q^3 tetrahedron, and 1,175 cm^{-1} was assigned to typical bands of Q^4 tetrahedron, respectively [31,32]. It is worth noting that these sub-peaks shifted and varied slightly in other samples, likely due to the fitting error and the potential chemical reaction/change during the hydration process of LCC samples. The intensity (proportion of relative area) of the Si–O (Q^3) bond in all GO-LCC paste decreased along with the increase of GO (Figure 7b), whereas the intensity of Q^4 increased (Figure 7c), indicating that GO converted more Q^3 into Q^4 [33]. The transformation from Q^3 to Q^4 corresponds to the generation of more complex hydrates.

Yang *et al.* [34] reached a similar conclusion in their study on GO-OPC binders from a nuclear magnetic resonance (NMR) perspective. Their findings provide additional evidence to support the deconvolved FTIR analysis conducted in this study. After 28 days of curing, it was observed that in the OPC binder, more Q^0 structures were transformed into higher-polymerized Si–O tetrahedra (Q^1 and Q^2) in the presence of GO. Specifically, the inclusion of 0.15 and 0.2 wt% of GO led to an increase in the mean chain length by 3.5 and 1.9%, respectively, suggesting the generation of more complex hydration products.

Figure 8 reveals the various carbonated phases in the hydrated LCC paste, demonstrating the influence of GO on the carbonation behavior of LCC paste samples. Generally, Ca-based carbonate could be divided into calcite, aragonite, and vaterite, which are characteristic of different FTIR patterns (Figure 8a), as verified by Chakrabarty and Mahapatra [35]. In this study, the calcite mainly came from the admixed limestone and the carbonated portlandite [31], whereas the aragonite and vaterite mainly came from the carbonated C–S–H/C–A–S–H. The unique two peaks (700

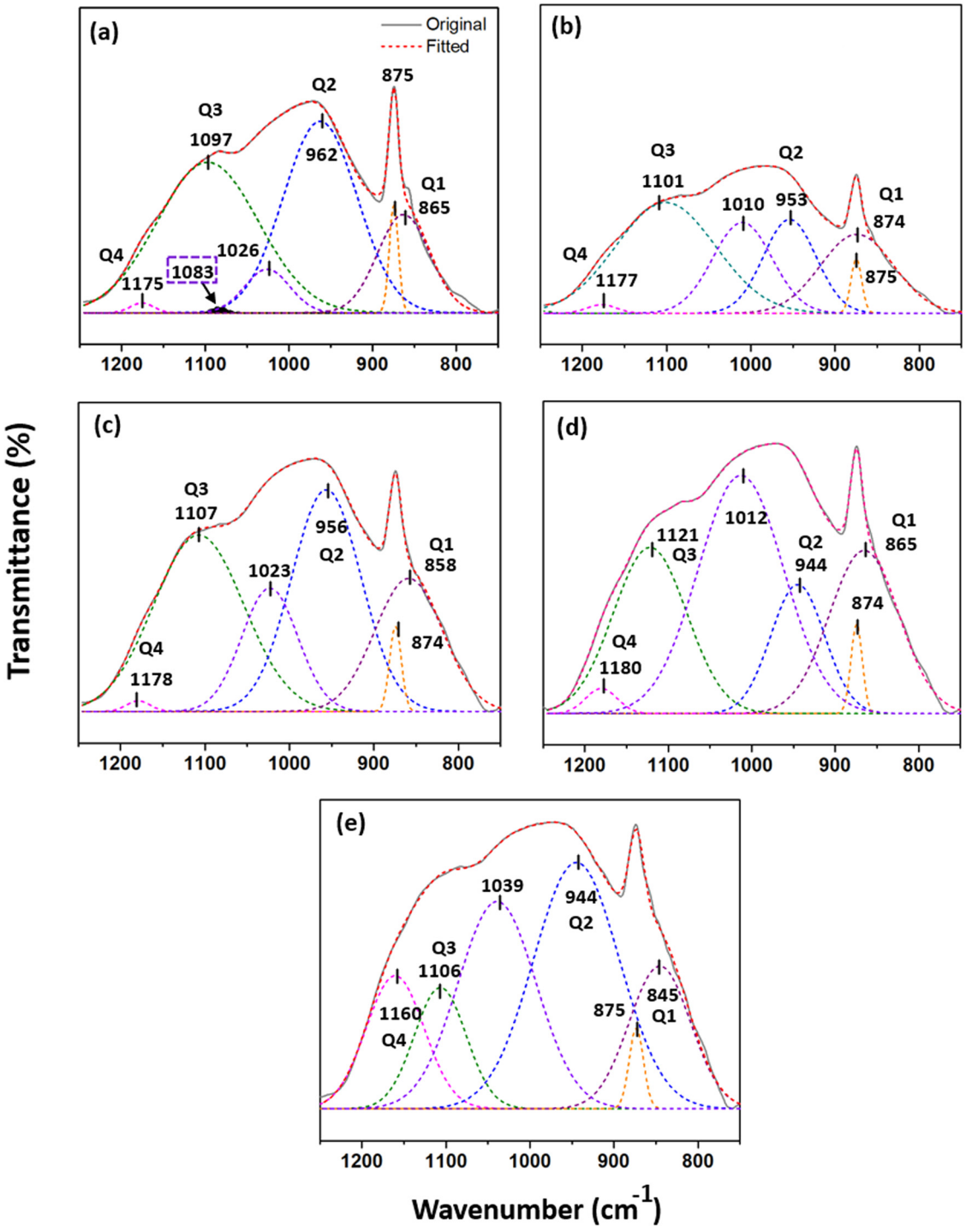

Figure 6: Deconvoluted FTIR patterns of selected GO-LCC paste samples from 750 to 1,250 cm^{-1} wavenumber length: (a) no-GO, (b) 0.045% GO, (c) 0.090% GO, (d) 0.135% GO, and (e) 0.180% GO. Note: due to the potential chemical reaction and fitting error, the center location for each sub-peak was slightly different.

and 712 cm^{-1}) of aragonite were not observed after admixing GO (Figure 8b), suggesting that during the carbonation of LCC paste in the air, the presence of GO mitigated the formation of unstable orthorhombic crystal systemic aragonite but facilitated the formation of stable trigonal crystal systemic calcite. This result was also confirmed by XRD analysis (Figure 8c) in which the intensity of aragonite in 0.09% GO-LCC was weaker than its counterpart without the admixed

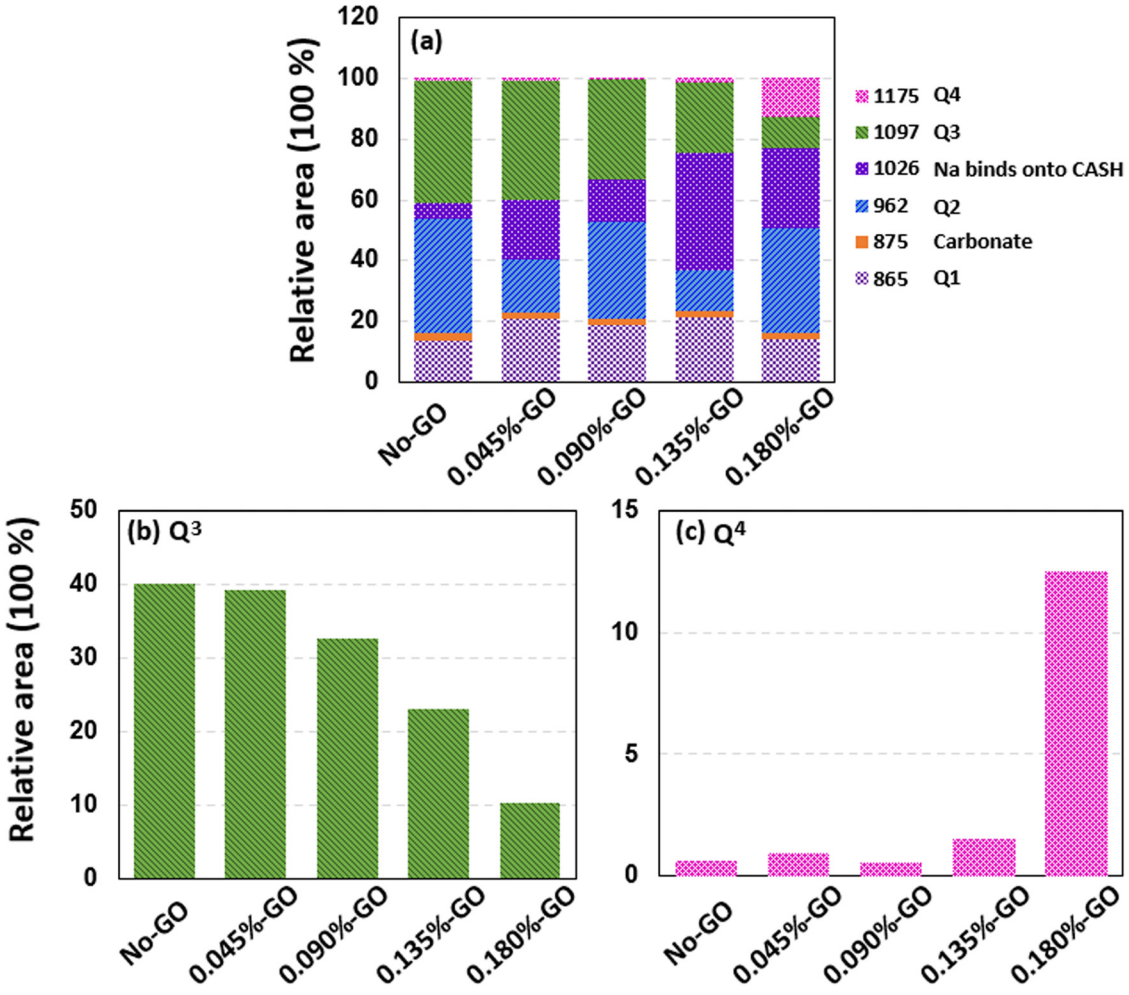

Figure 7: (a) Relative area of deconvoluted sub-peaks from 750 to 1,250 cm^{-1} wavenumber length, (b) the relative area of Q^3 (1,097 cm^{-1}), and (c) the relative area of Q^4 (1,175 cm^{-1}). Note: due to the bond shift and fitting error, the center location for each sub-peak was slightly different.

GO. The quantification of carbonate phases will be discussed in the TGA/DTG section later.

The XRD analysis also sheds light on the hydration process of selected LCC binders. Compared with the original no-GO LCC paste, the intensity of peaks in 0.09%-GO LCC paste at about 18° ($Ca(OH)_2$), 34°($Ca(OH)_2$), 36°($CaCO_3$), 39°(Quartz), and 48°(kaolinite) decreased [32,36,37], suggesting that these components were consumed due to participation in the binder hydration process. In other words, the admixed GO accelerated the hydration process of LCC paste. This conclusion is consistent with our previous work that GO accelerated the hydration process of both OPC and geopolymer binder [11,17]. Furthermore, Lin *et al.* reported enhanced carbonation resistance of the LC^3 binder by introducing nano-silica, as observed in a laboratory accelerated carbonation test. Their research primarily focuses on the denser microstructure induced by nano-silica.

3.4 SEM analysis

Figure 9 illustrates the microstructure of 0.09 wt% GO-LCC paste and its control sample (no-GO) at 28-day curing age, aimed to evaluate the influence of GO on the morphology of hydrates of LCC paste. As shown in Figure 9a and b, the microstructure of 0.09 wt% GO-LCC paste is denser than the control sample and seems to have fewer defects, suggesting the beneficial effects of GO on the microstructure of LCC paste. Note that denser microstructure tends to translate to higher compressive performance as well as better durability performance (through lower water absorption, lower gas permeability, and lower diffusivity of detrimental ions). Our previous research also demonstrated similar results; specifically, the admixed GO facilitated more homogenous layer-by-layer hydrates in a fly ash-based geopolymer paste while the unmodified geopolymer

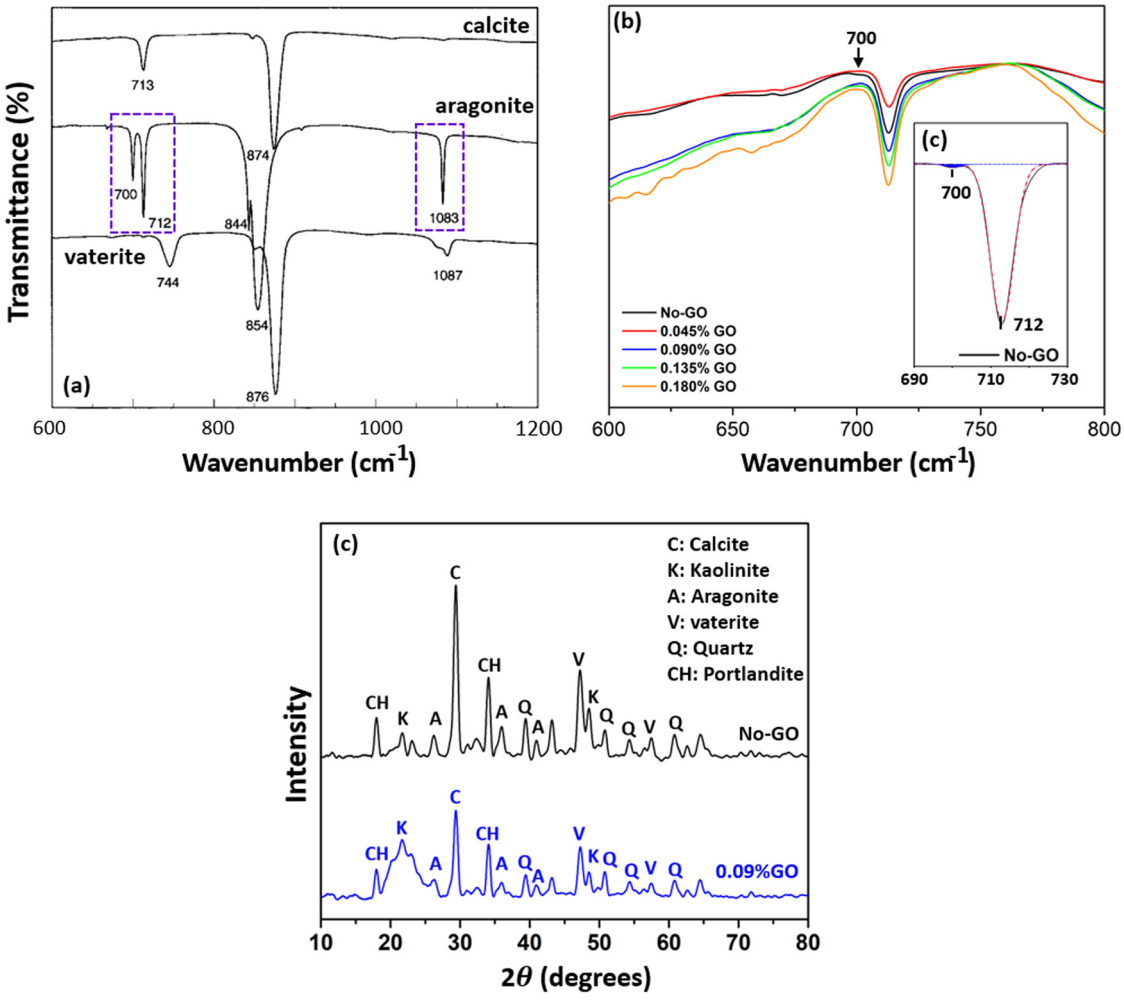

Figure 8: (a) FTIR patterns of calcite, aragonite, and vaterite [35], (b) the weak two-peak (700 and 712 cm^{-1}) verified the presence of aragonite, and (c) the XRD patterns of original LCC paste and 0.09% GO LCC paste.

featured loose and disordered hydrates [11]. This phenomenon was also known as the "hydrate growth template effect." This effect primarily stemmed from the interaction between chemical functional groups (such as C–OH) present on the surface of GO and the chemical constituents of hydrates. This interaction facilitated the generation of a layered structure through a sequential process. A comparable outcome has been observed in the current study as well (Figure 9c).

More obvious differences were detected in SEM at the magnification of 20,000 times (Figure 9c and d), where the 0.09 wt% GO-LCC paste exhibits a more homogenous and denser microstructure. It is well known that the morphology of cementitious hydrates (*e.g.*, C–S–H and C–A–S–H) mainly depends on the molar ratio of key elements (especially Ca/Si, S/Al, and Ca/(Si + Al)). The more uniform the molar ratio of key elements, the more consistent the polymerization degree of binder hydrates, and the more homogenous the hydration products [5]. Therefore, the homogeneous hydrates in this study indicate that the admixed GO facilitated a more uniform distribution of key elements. In other words, the presence of GO reduced the variability in the polymerization degree of the LCC binder, as suggested by the positive correlation between Ca/Si (or Ca/(Si + Al)) and hydration polymerization degree [38].

The aforementioned advantages of GO likely resulted from the functional groups on the surface of GO, which provide the GO nanosheets with a significant negative charge. The GO nanosheets thus serve as templates to attract cations (*e.g.*, Ca^{2+}, Na^{+}, and K^{+}). The cations can then react with Si, Al, and S species to form hydration products (such as C–S–H, C–A–S–H, AFt, and AFm). In summary, the GO guided the hydration of the cementitious binder and led to a more integrated microstructure and better compressive strengths. Lv *et al.* [20] reported similar results that the admixed GO induced homogeneous flower-like hydrates in

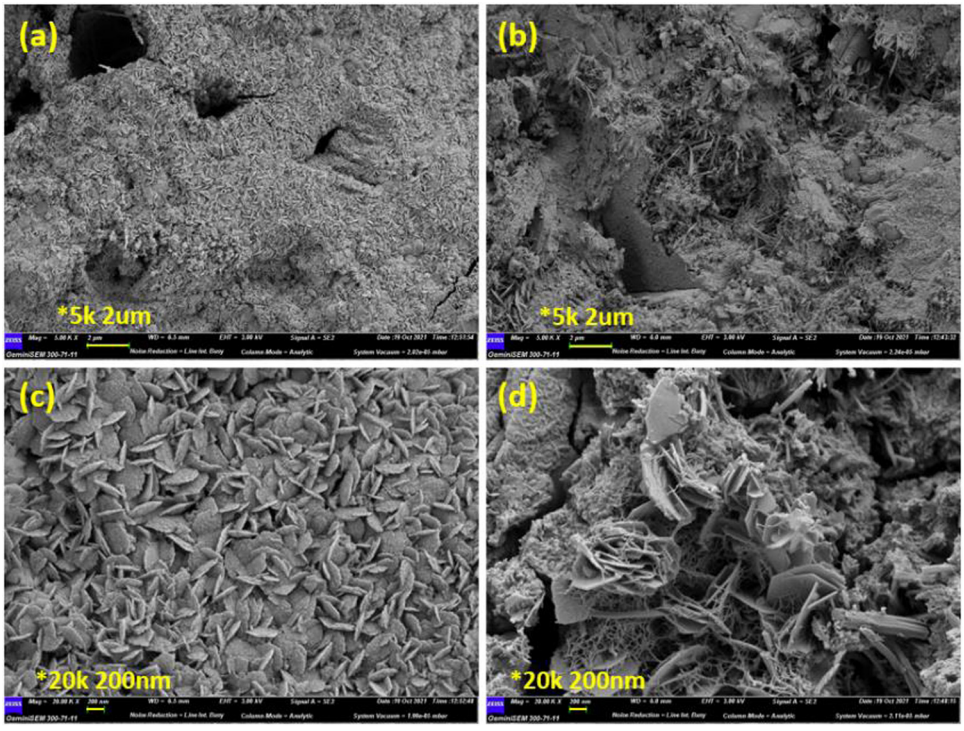

Figure 9: SEM results of (a) 0.09 wt% GO-LCC paste and (b) control sample at the magnification of 5k times; and (c) 0.09 wt% GO-LCC paste and (d) control sample at the magnification of 20k times.

an OPC paste matrix. In addition, Lv *et al.* detailed the template mechanism of GO, which is also responsible for the homogenous hydrates observed in this study.

3.5 Thermogravimetric and differential thermal analysis

Figure 10 illustrates the thermogravimetric-differential thermal analysis results of selected GO-LCC paste samples, which help elucidate the influence of GO on the hydration products of LCC paste. As shown in Figure 10, this first mass loss was detected between 50 and 150°C, corresponding to the escape of the residual water, the decomposition of AFt (Ettringite) and AFm, and the dehydration of partial C–S–H/C–A–S–H. It was clear that the admixed GO mitigated the generation of AFt, inspiring the potential use of GO to mitigate the risk of delayed ettringite formation in heat-cured concrete [39] or mass concrete. Xu *et al.* also demonstrated a similar result by analyzing the key elemental information obtained by electron

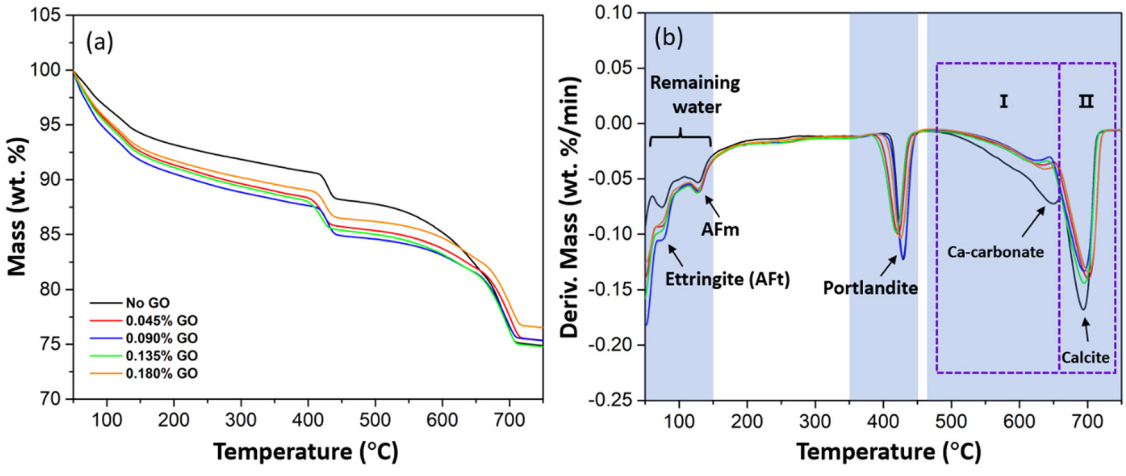

Figure 10: (a) TGA and (b) DTG analysis of selected GO-LCC paste.

probe microanalysis; specifically, they reported that 0.02 wt% GO facilitated the transformation from AFt to other Al-rich phases [17].

The second mass loss in Figure 10 was detected between 350 and 450°C, corresponding to the decomposition of portlandite. The DTG peak of portlandite in the curve of 0.09 wt% GO-LCC paste was sharper than in other samples, suggesting that the admixed GO induced the formation of more and better crystallized portlandite. This result agrees with the study by Mokhtar *et al.* [40] in which GO induced a higher content of portlandite in OPC binder and they attributed this higher content of portlandite to the GO-accelerated hydration process of OPC. Yang *et al.* also reported that the content of portlandite was slightly increased along with the increment of GO dosage in OPC binder [34].

The last mass loss in Figure 10 was detected between 450 and 750°C, corresponding to the decomposition of carbonate. It was clear that the admixed GO mitigated the carbonation of the LCC paste, because 0.045, 0.090, 0.135, and 0.180% GO decreased the relative amount of total carbonate by about 19.7, 25.1, 17.5, and 23.6%, respectively. This result agreed well with our previous work that the admixed GO improved the carbonation resistance of an OPC paste [17].

It is noteworthy that the third main mass loss consists of multiple peaks, suggesting that multiple decompositions or transformations occurred simultaneously. As confirmed by FTIR, two other types of Ca-carbonates: vaterite and aragonite, were also detected in the carbonated LCC paste. Both of them not only decomposed in the temperature range I (Figure 10b) but also transformed into calcite and then decomposed in the temperature range II [41], which made the quantification of each component much more complex.

4 Concluding remarks

This work proposed an innovative strategy to employ GO to enhance unconventional LCC paste. To elucidate the mechanistic roles played by GO in the LCC paste system, this laboratory study explored the influence of GO on the compressive strength and flowability of the designed paste, and the microscopic investigation further shed light on the microscopic change of LCC paste induced by GO. The main conclusions are drawn as follows:

1) GO effectively improved the compressive strength of LCC paste samples. The optimal dosage of GO in this study was 0.09% by weight of the LCC paste, which improved the compressive strength at 7, 14, and 28 s by 25.6, 21.6, and 20.3%, respectively. However, when the dosage of GO exceeded 0.09 wt%, the benefit to the compressive strength of the LCC paste declined, likely due to undesirable agglomeration of GO and pores resulted from GO-accelerated hydration of LCC. In addition, the admixed GO reduced the flowability of fresh LCC paste, due to the accelerated hydration of LCC induced by GO. These results provide a promising strategy for engineers to enhance the performance of LCC paste in the field while balancing the constructability of the fresh concrete and the mechanical properties of the hardened concrete.
2) GO played several critical roles in the LCC paste. It served as the hydration growth templates and regulated the hydrates, as evidenced by the layer-by-layer hydrate structures observed in SEM. GO also accelerated the hydration process, as indicated by the presence of more crystalline portlandite phases, as shown by TGA, and the consumption of more mineral phases, as demonstrated by XRD. GO improved the polymerization degree of hydrates, as evidenced by a higher content of complex hydrates observed in FTIR. Moreover, GO enhanced the carbonation resistance of hydrates, as supported by the various carbon-related peaks observed in FTIR and TGA. In addition, GO converted the unstable orthorhombic crystal systemic aragonite to the stable trigonal crystal systemic calcite. All these roles are similar to the roles played by GO in cement and geopolymer binders.

Future work should further investigate the fundamentals underlying the mechanical properties and durability performance of GO-modified LCC composites, using advanced tools (*e.g.*, nanoindentation and NMR spectroscopy), to offer in-depth insights and fundamental understanding. Additional research may also explore the use of higher content of calcined clay and limestone (*i.e.*, lower content of cement) to further greening the LCC technology with the aid of nanotechnology. While this study did not directly assess the durability performance, the results suggest that the admixed GO is beneficial to the durability of LCC composites, including slowing down the ingress of moisture, gases, and detrimental ions (in light of the denser microstructure), and improving chemical resistances (in light of the higher polymerization degree of hydrates).

Funding information: This work was financially supported by the Key Laboratory of Catalysis and Energy Materials Chemistry of Ministry of Education & Hubei Key Laboratory of Catalysis and Materials Science (Project # CHCL19001), Hubei Provincial Department of Construction (Construction Science and Technology Plan Project 2019-672-3-3), and Hubei Provincial Department of Construction (Construction Science and Technology Plan Project 2021-28-56).

Author contributions: Jing Gong: writing – original draft, funding acquisition, validation, methodology, data collection, data curation, conceptualization; Yi Qian: writing – original draft, data curation; Ziyang Xu: validation, methodology, data collection, data curation; Chaoqian Chen: data curation; Yijing Jin: data curation; Junze Zhang: data curation; Zhipeng Li: writing – review and editing, validation, methodology, conceptualization; Xianming Shi: writing – review and editing, supervision, conceptualization. All authors have accepted the responsibility for the entire content of this manuscript and approved its submission.

Conflict of interest: The authors state no conflict of interest.

References

[1] Benhelal E, Zahedi G, Shamsaei E, Bahadori A. Global strategies and potentials to curb CO_2 emissions in cement industry. J Clean Prod. 2013;51:142–61.

[2] Sharma M, Bishnoi S, Martirena F, Scrivener K. Limestone calcined clay cement and concrete: a state-of-the-art review. Cem Concr Res. 2021;149:106564.

[3] Scrivener K, Martirena F, Bishnoi S, Maity S. Calcined clay limestone cements (LC3). Cem Concr Res. 2018;114:49–56.

[4] Nguyen QD, Afroz S, Castel A. Influence of calcined clay reactivity on the mechanical properties and chloride diffusion resistance of limestone calcined clay cement (LC3) concrete. J Mar Sci Eng. 2020;8(5):301.

[5] Li Z, Fei ME, Huyan C, Shi X. Nano-engineered, fly ash-based geopolymer composites: an overview. Resour Conserv Recycl. 2021;168:105334.

[6] Li Z, Gong J, Du S, Wu J, Li J, Hoffman D, et al. Nano-montmorillonite modified foamed paste with a high volume fly ash binder. RSC Adv. 2017;7(16):9803–12.

[7] Antoni M, Rossen J, Martirena F, Scrivener K. Cement substitution by a combination of metakaolin and limestone. Cem Concr Res. 2012;42(12):1579–89.

[8] Drissi S, Shi C, Li N, Liu Y, Liu J, He P. Relationship between the composition and hydration-microstructure-mechanical properties of cement-metakaolin-limestone ternary system. Constr Build Mater. 2021;302:124175.

[9] Vaasudevaa BV, Dhandapani Y, Santhanam M. Performance evaluation of limestone-calcined clay (LC2) combination as a cement substitute in concrete systems subjected to short-term heat curing. Constr Build Mater. 2021;302:124121.

[10] Li Z, Zhang Z, Fei ME, Shi X. Upcycling waste mask PP microfibers in portland cement paste: surface treatment by graphene oxide. Mater Lett. 2022;318:132238.

[11] Li Z, Shi X. Graphene oxide modified, clinker-free cementitious paste with principally alkali-activated fly ash. Fuel. 2020;269:117418.

[12] Gao Y, Luo J, Yuan S, Zhang J, Gao S, Zhu M, et al. Fabrication of graphene oxide/fiber reinforced polymer cement mortar with remarkable repair and bonding properties. J Mater Res Technol. 2023;24:9413–33.

[13] Li D, Müller MB, Gilje S, Kaner RB, Wallace GG. Processable aqueous dispersions of graphene nanosheets. Nat Nanotech. 2008;3(2):101–5.

[14] Gao Y, Luo J, Zhang J, Zhou X, Teng F, Liu C, et al. Repairing performances of novel cement mortar modified with graphene oxide and polyacrylate polymer. Nanotechnol Rev. 2022;11(1):1778–91.

[15] Luo J, Zhou C, Li W, Chen S, Korayem AH, Duan W. Using graphene oxide to improve physical property and control ASR expansion of cement mortar. Constr Build Mater. 2021;307:125006.

[16] Luo J, Chen S, Li Q, Liu C, Gao S, Zhang J, et al. Influence of graphene oxide on the mechanical properties, fracture toughness, and microhardness of recycled concrete. Nanomaterials. 2019;9(3):325.

[17] Xu G, Du S, He J, Shi X. The role of admixed graphene oxide in a cement hydration system. Carbon. 2019;148:141–50.

[18] Pan Z, He L, Qiu L, Du S, Korayem A, Li G, Zhu J, et al. Mechanical properties and microstructure of a graphene oxide–cement composite. Cement and Concrete Composites. 2015;58:140–47.

[19] Tang Z, Li Z, Fan L, Gong J, Zhong J, Shi X. Effect of surface tension, foaming stabilizer, and graphene oxide on the properties of foamed paste. J Nanosci Nanotechnol. 2021 May;21(5):3123–33.

[20] Lv S, Ma Y, Qiu C, Sun T, Liu J, Zhou Q. Effect of graphene oxide nanosheets of microstructure and mechanical properties of cement composites. Constr Build Mater. 2013;49:121–7.

[21] Lin RS, Oh S, Du W, Wang XY. Strengthening the performance of limestone-calcined clay cement (LC3) using nano silica. Constr Build Mater. 2022;340:127723.

[22] Chuah S, Li W, Chen SJ, Sanjayan JG, Duan WH. Investigation on dispersion of graphene oxide in cement composite using different surfactant treatments. Constr Build Mater. 2018;161:519–27.

[23] Li Z, Xu G, Shi X. Reactivity of coal fly ash used in cementitious binder systems: a state-of-the-art overview. Fuel. 2021;301:121031.

[24] Luo Y, Wu Y, Ma S, Zheng S, Zhang Y, Chu PK. Utilization of coal fly ash in China: a mini-review on challenges and future directions. Env Sci Pollut Res. 2021;28(15):18727–40.

[25] Lu Z, Li X, Hanif A, Chen B, Parthasarathy P, Yu J, et al. Early-age interaction mechanism between the graphene oxide and cement hydrates. Constr Build Mater. 2017;152:232–9.

[26] An J, Nam BH, Alharbi Y, Cho BH, Khawaji M. Edge-oxidized graphene oxide (EOGO) in cement composites: cement hydration and microstructure. Compos Part B: Eng. 2019;173:106795.

[27] Li R, Ye H. Influence of alkalis on natural carbonation of limestone calcined clay cement pastes. Sustainability. 2021;13(22):12833.

[28] Ylmén R, Jäglid U, Steenari BM, Panas I. Early hydration and setting of Portland cement monitored by IR, SEM and Vicat techniques. Cem Concr Res. 2009 May;39(5):433–9.

[29] Gong J, Yu L, Li Z, Shi X. Mechanical activation improves reactivity and reduces leaching of municipal solid waste incineration (MSWI) bottom ash in cement hydration system. J Clean Prod. 2022;363:132533.

[30] Zhang J, Shi C, Zhang Z. Carbonation induced phase evolution in alkali-activated slag/fly ash cements: the effect of silicate modulus of activators. Constr Build Mater. 2019;223:566–82.

[31] Morandeau A, Thiéry M, Dangla P. Investigation of the carbonation mechanism of CH and C-S-H in terms of kinetics, microstructure changes and moisture properties. Cem Concr Res. 2014;56:153–70.

[32] Zentar R, Wang D, Abriak NE, Benzerzour M, Chen W. Utilization of siliceous–aluminous fly ash and cement for solidification of marine sediments. Constr Build Mater. 2012;35:856–63.

[33] Kupwade-Patil K, Palkovic SD, Bumajdad A, Soriano C, Büyüköztürk O. Use of silica fume and natural volcanic ash as a replacement to Portland cement: micro and pore structural investigation using NMR, XRD, FTIR and X-ray microtomography. Constr Build Mater. 2018;158:574–90.
[34] Yang H, Monasterio M, Cui H, Han N. Experimental study of the effects of graphene oxide on microstructure and properties of cement paste composite. Compos Part A: Appl Sci Manuf. 2017;102:263–72.
[35] Chakrabarty D, Mahapatra S. Aragonite crystals with unconventional morphologies. J Mater Chem. 1999;9(11):2953–7.
[36] Lin RS, Han Y, Wang XY. Macro–meso–micro experimental studies of calcined clay limestone cement (LC3) paste subjected to elevated temperature. Cem Concr Compos. 2021;116:103871.
[37] Maraghechi H, Avet F, Wong H, Kamyab H, Scrivener K. Performance of limestone calcined clay cement (LC3) with various kaolinite contents with respect to chloride transport. Mater Struct. 2018;51(5):125.
[38] Davidovits J. Mineral polymers and methods of making them [Internet]. US4349386A; 1982 [cited 2022 Aug 18]. https://patents.google.com/patent/US4349386A/en.
[39] Kawabata Y, Ueda N, Miura T, Multon S. The influence of restraint on the expansion of concrete due to delayed ettringite formation. Cem Concr Compos. 2021;121:104062.
[40] Mokhtar MM, Abo-El-Enein SA, Hassaan MY, Morsy MS, Khalil MH. Mechanical performance, pore structure and micro-structural characteristics of graphene oxide nano platelets reinforced cement. Constr Build Mater. 2017;138:333–9.
[41] Tone T, Koga N. Thermally induced aragonite–calcite transformation in freshwater pearl: A mutual relation with the thermal dehydration of included water. ACS Omega. 2021;6(21):13904–14.